

Revision 1

Lead-antimony sulfosalts from Tuscany (Italy). XVIII. New data on the crystal-chemistry of boscardinite

CRISTIAN BIAGIONI^{1*}, YVES MOËLO²

¹ *Dipartimento di Scienze della Terra, Università di Pisa, Via S. Maria 53, I-56126 Pisa, Italy*

² *Institut des Matériaux Jean Rouxel, UMR 6502, CNRS, Université de Nantes, 2, rue de la Houssinière, 44322 Nantes Cedex 3, France*

*e-mail address: biagioni@dst.unipi.it

ABSTRACT

16
17 Boscardinite, ideally $\text{TlPb}_4(\text{Sb}_7\text{As}_2)_{\Sigma 9}\text{S}_{18}$, has been recently described as a new homeotypic
18 derivative of baumhauerite, found at Monte Arsiccio mine, Apuan Alps, Tuscany, Italy. New
19 findings of boscardinite in different mineral associations of this deposit allowed the collection
20 of new crystal chemical data. Electron-microprobe analysis of the crystal used for the single-
21 crystal X-ray diffraction study gave (in wt%): Ag 1.81(5), Tl 12.60(21), Pb 17.99(12), Hg
22 0.14(5), As 9.36(12), Sb 33.60(27), S 23.41(30), Cl 0.06(1), total 98.97(100). On the basis of
23 $\Sigma Me = 14$ apfu, it corresponds to $\text{Ag}_{0.42}\text{Tl}_{1.52}\text{Pb}_{2.14}\text{Hg}_{0.02}(\text{Sb}_{6.82}\text{As}_{3.08})_{\Sigma 9.90}\text{S}_{18.04}\text{Cl}_{0.04}$. With
24 respect to the type specimen, these new findings are characterized by a strong Pb depletion,
25 coupled with higher Tl contents, and a significant As enrichment. The single-crystal X-ray
26 diffraction study of this (Tl,As)-enriched boscardinite confirms the structural features
27 described for the type sample. The unit-cell parameters are $a = 8.1017(4)$, $b = 8.6597(4)$, $c =$
28 $22.5574(10)$ Å, $\alpha = 90.666(2)$, $\beta = 97.242(2)$, $\gamma = 90.850(2)^\circ$, $V = 1569.63(12)$ Å³, space
29 group $P\bar{1}$. The crystal structure was refined down to $R_1 = 0.0285$ on the basis of 6582
30 reflections with $F_o > 4\sigma(F_o)$. Arsenic is dominant in three $Me\text{S}_3$ sites, against one in type
31 boscardinite. The main As-enrichment is observed in the sartorite-type sub-layer. Owing to
32 this chemical peculiarity, (Tl,As)-rich boscardinite shows the alternation, along **b**, of Sb-rich
33 sites and As-rich sites; this feature represents the main factor controlling the 8 Å
34 superstructure. The chemical variability of boscardinite is discussed; the Ag increase observed
35 here gets closer to stoichiometric $\text{AgTl}_3\text{Pb}_4(\text{Sb}_{14}\text{As}_6)_{\Sigma 20}\text{S}_{36}$ ($Z = 1$), against possible extension
36 up to $\text{AgTl}_2\text{Pb}_6(\text{Sb}_{15}\text{As}_4)_{\Sigma 19}\text{S}_{36}$ for type boscardinite.

37

38 *Key-words:* boscardinite, sartorite homologous series, thallium, silver, sulfosalt, Monte
39 Arsiccio mine, Apuan Alps, Tuscany, Italy.

40

41 Introduction

42 Boscardinite, ideally $\text{TlPb}_4(\text{Sb}_7\text{As}_2)_{\Sigma 9}\text{S}_{18}$, is a $N = 3.5$ member of the sartorite
 43 homologous series (Makovicky, 1985). It is the (Tl,Sb)-homeotype of baumhauerite, first
 44 described by Orlandi *et al.* (2012) from the Sant’Olga level, Monte Arsiccio mine, Apuan
 45 Alps, Tuscany, Italy. In the type material boscardinite occurs as mm-sized lead grey compact
 46 metallic masses embedded in a quartz vein, in association with zinkenite. A second
 47 occurrence of boscardinite has been described by Topa *et al.* (2013) in intimate intergrowth
 48 with stibnite and smithite from the Jas Roux thallium mineralization, Hautes-Alpes, France.

49 After the first finding of boscardinite in a quartz vein (occurrence of Type 3 in
 50 agreement with Biagioni *et al.*, 2014b) embedded in the dolostone from the Sant’Olga level,
 51 new specimens of boscardinite-like sulfosalts have been found in the microcrystalline baryte
 52 + pyrite ore bodies, at the contact between schist and dolostone (Type 1 occurrence) and in
 53 the pyrite-rich dolostone (Type 2 occurrence). In particular, in this latter kind of occurrence,
 54 boscardinite is associated with protochabournéite and routhierite, forming compact black
 55 masses up to 1 cm in size. The chemical characterization of these new specimens of
 56 boscardinite pointed out some peculiarities and, in particular, a strong Pb depletion, coupled
 57 with higher Tl contents, and a significant As enrichment. Consequently, a structural study was
 58 performed.

59 A similar chemistry was observed in an additional specimen of boscardinite collected
 60 in the Sant’Anna level, an upper underground level of the Monte Arsiccio mine. In this further
 61 specimen, boscardinite occurs in thin veinlets within a grey dolostone, intimately associated
 62 with a “protochabournéite-like” mineral and small red grains of cinnabar.

63 The aim of this paper is to contribute to the knowledge of the crystal chemistry of
 64 sartorite homologues and, in particular, of the (Tl,Sb)-homeotypic derivative of baumhauerite.

66 Experimental

67 Chemical analysis

68 Two specimens of boscardinite from the Sant’Olga (sample #408) and the Sant’Anna
 69 levels (sample #2) were analyzed with a CAMEBAX SX100 electron microprobe. The
 70 operating conditions were: accelerating voltage 20 kV, beam current 20 nA, beam size 1 μm .
 71 Standards (element, *emission line*, counting times for one spot analysis) are: galena (Pb $M\alpha$,
 72 60 s), stibnite (Sb $L\alpha$, 60 s), AsGa (As $L\alpha$, 30 s), pyrite (S $K\alpha$, 60 s), Ag (Ag $L\alpha$, 30 s),
 73 lorándite (Tl $M\alpha$, 20 s), cinnabar (Hg $M\alpha$, 20 s), and pyromorphite (Cl $K\alpha$, 30 s). Results are
 74 given in Table 1. On the basis of $\Sigma Me = 14$ atoms per formula unit (*apfu*), the corresponding
 75 chemical formulae are $\text{Ag}_{0.42}\text{Tl}_{1.52}\text{Hg}_{0.02}\text{Pb}_{2.14}(\text{Sb}_{6.82}\text{As}_{3.08})_{\Sigma 9.90}\text{S}_{18.04}\text{Cl}_{0.04}$ and
 76 $\text{Ag}_{0.34}\text{Tl}_{1.41}\text{Hg}_{0.02}\text{Pb}_{2.51}(\text{Sb}_{6.95}\text{As}_{2.78})_{\Sigma 9.73}\text{S}_{18.04}\text{Cl}_{0.04}$ for samples #408 and #2, respectively.
 77 Each of the two groups of analytical data is very homogeneous. The $\text{As}/(\text{As}+\text{Sb})_{\text{at}}$ ratio is
 78 0.31 and 0.29 for samples #408 and #2, respectively, to be compared with the values 0.21 and
 79 0.24 for samples #4977 and #4989 described by Orlandi *et al.* (2012). Moreover, the
 80 $\text{Pb}/(\text{Pb}+2\text{Tl})_{\text{at}}$ ratios are 0.41 (#408) and 0.47 (#2), to be compared with 0.54 (#4977) and
 81 0.59 (#4989). Thus, the new specimens of boscardinite are (Tl,As)-richer than type
 82 boscardinite.

83 Applying the substitutions $\text{Hg}^{2+} + \text{Pb}^{2+} = \text{Ag}^+ + \text{Sb}^{3+}$, $\text{Ag}^+ + \text{Sb}^{3+} = 2\text{Pb}^{2+}$, and $\text{Pb}^{2+} +$
 84 $\text{Cl}^- = \text{Sb}^{3+} + \text{S}^{2-}$, the following formulae can be obtained: $\text{Tl}_{1.52}\text{Pb}_{2.96}(\text{Sb}_{6.44}\text{As}_{3.08})_{\Sigma 9.52}\text{S}_{18.08}$
 85 (sample #408) and $\text{Tl}_{1.41}\text{Pb}_{3.17}(\text{Sb}_{6.65}\text{As}_{2.78})_{\Sigma 9.43}\text{S}_{18.08}$ (sample #2). They are close to the
 86 simplified formula $\text{Tl}_{1.5}\text{Pb}_3(\text{Sb}_{6.5}\text{As}_3)_{\Sigma 9.5}\text{S}_{18}$.

87 *Single-crystal X-ray diffraction*

89 The sample #408, being the richest in Tl and As between the two new studied samples,
 90 was used for the single-crystal X-ray diffraction study. Intensity data were collected using a
 91 Bruker Smart Breeze diffractometer equipped with an air-cooled CCD detector, with Mo $K\alpha$
 92 radiation. The detector-to-crystal distance was 60 mm. 4896 frames were collected using ω
 93 and ϕ scan modes, in 0.25° slices, with an exposure time of 45 seconds per frame. The data
 94 were corrected for the Lorentz and polarization factors and absorption using the package of
 95 software *Apex2* (Bruker AXS Inc., 2004). The statistical tests on the distribution of $|E|$ values
 96 ($|E^2 - 1| = 0.981$) and the systematic absences are consistent with the space group $P\bar{1}$. The
 97 refined unit-cell parameters are $a = 8.1017(4)$, $b = 8.6597(4)$, $c = 22.5574(10)$ Å, $\alpha =$
 98 $90.666(2)$, $\beta = 97.242(2)$, $\gamma = 90.850(2)^\circ$, $V = 1569.63(12)$ Å³.

99 The crystal structure was refined using *Shelxl-97* (Sheldrick, 2008) starting from the
 100 atomic coordinates of boscardinite given by Orlandi *et al.* (2012). Scattering curves for
 101 neutral atoms were taken from the *International Tables for Crystallography* (Wilson, 1992).
 102 Crystal data and details of the intensity data collection and refinement are reported in Table 2.
 103 The site occupation factor (s.o.f.) of mixed (Sb/As) and (Sb/Ag) sites was freely refined using
 104 the scattering curves of Sb vs As and Sb vs Ag, respectively. On the contrary, the s.o.f. of
 105 mixed (Tl/Pb) sites was fixed on the basis of bond-valence calculations, owing to the
 106 similarity between the site scattering values of Tl and Pb. After several cycles of isotropic
 107 refinement, the R_1 converged to 0.097, thus confirming the correctness of the structural
 108 model. The isotropic displacement parameter at the Pb3 and Pb4 sites proved to be relatively
 109 high, suggesting the replacement of (Pb,Tl) by a lighter atom, *i.e.* Sb. The s.o.f. of these two
 110 sites was refined using the scattering curves Pb vs Sb, freely refining their coordinates; the R_1
 111 factor lowered to 0.077. By introducing the anisotropic displacement parameters for all cation
 112 positions made the refinement to converge to $R_1 = 0.038$. Finally, an anisotropic model for all
 113 the atom positions lowered the final R_1 value to 0.028 for 6582 reflections with $F_o > 4\sigma(F_o)$
 114 and 0.033 for all 7211 independent reflections. The highest and deepest residuals are located
 115 around Pb3 and Pb4 sites, respectively. Atomic coordinates and selected bond distances are
 116 reported in Table 3 and Table 4, respectively. Bond valence sums are given in Table 5.

117 **Crystal structure of (Tl,As)-enriched boscardinite**

118 *General features, cation coordination, and site occupancies*

119 The general organization of the crystal structure fully agrees with that described by
 120 Orlandi *et al.* (2012) for boscardinite (Fig. 1). This mineral, belonging to the sartorite
 121 homologous series, is formed by the 1:1 alternation, along **c**, of a sartorite-type layer ($N = 3$)
 122 and a dufrénoysite-type layer ($N = 4$), connected by zig-zag chains of (Pb,Tl,Sb) atoms
 123 running along **a**. Sartorite layers are flanked by Tl sites, hosting minor Pb, whereas the
 124 dufrénoysite layer is flanked by mixed and split (Pb/Sb) sites. It should be noted that the
 125

126 sartorite layers in type boscardinite are flanked by alternating (Tl,Pb) and (Pb,Tl) sites,
 127 whereas the dufrénoysite layers are flanked by pure Pb and mixed (Pb,Tl) sites.

128 Within the layers, mixed (Sb/As) sites, with various $(As/Sb)_{at}$ ratios, occur. Owing to
 129 the higher $As/(As+Sb)_{at}$ ratio with respect to the type boscardinite, pure Sb sites are
 130 accompanied by mixed (Sb/As) sites, either Sb- or As-dominant. Within the dufrénoysite type
 131 layer, the same kind of alternation along **b** of one (Sb/Pb) site and one (Ag/Sb) site occurs,
 132 similar to the configuration observed in rathite (Berlepsch *et al.*, 2002), barikaite (Makovicky
 133 and Topa, 2013), and carducciite (Biagioni *et al.*, 2014c).

134 Cation coordinations correspond to those described by Orlandi *et al.* (2012) for type
 135 boscardinite. Bond-valence sums (Table 5) are good; the most important deviations are
 136 represented by the valence deficit of the Sb atoms at the Sb3b and Sb4b sites, related to the
 137 ligand positions that are actually averaged S positions for the (Pb/Sb) mixture at those
 138 positions. Table 6 gives a comparison between site occupancies and average bond distances
 139 for type boscardinite and its (Tl,As)-enriched analogue. The most remarkable differences
 140 involve the cations forming the zig-zag chains of heavy atoms separating the dufrénoysite
 141 type layers from the sartorite type ones. In particular, the (Pb,Tl)_{2a}/(Pb,Tl)_{2b} split pair is
 142 replaced by two Tl_{2a} and Tl_{2b} split positions dominated by thallium, as shown by the larger
 143 average bond distances. This substitution possibly correlates with the occurrence of minor Sb
 144 at the Pb3 and Pb4 positions, which are split into two sub-positions (Pb3a/Sb3b) and
 145 (Pb4a/Sb4b), respectively. In type boscardinite, these sites have been modelled as a mixed
 146 (Pb,Tl)₃ and a pure Pb₄ site (see below).

147 Owing to the similar scattering factors for Tl and Pb, their s.o.f. was proposed on the
 148 basis of bond-valence calculation, by using, for the pair (Tl,S), the bond-valence parameter
 149 $R_{Tl,S}$ tabulated by Brese and O’Keeffe (1991), *i.e.* 2.63 Å, or alternatively, the value proposed
 150 by Biagioni *et al.* (2014a), *i.e.* 2.55 Å. Table 7 shows the s.o.f. of mixed (Tl/Pb) sites on the
 151 basis of the two proposed $R_{Tl,S}$ values in type boscardinite and in (Tl,As)-enriched
 152 boscardinite. The use of the bond-valence parameter given by Brese and O’Keeffe (1991)
 153 results in an underestimation of the Tl content in (Tl,As)-enriched boscardinite ($\Sigma Tl = 1.27$
 154 *apfu*, to be compared with 1.52 *apfu* obtained through electron-microprobe analysis). This
 155 underestimation does not apparently occur in type boscardinite, possibly owing to the fact that
 156 Orlandi *et al.* (2012) interpreted the low BVS at the Pb3 site as due to the occurrence of minor
 157 Tl. In (Tl,As)-rich boscardinite, this position is split into two partially occupied Pb and Sb
 158 sub-sites. The low BVS at the Pb3 site in type boscardinite could also be the result of an
 159 average position of this site. If so, the high Tl content obtained by using the BVS parameter of
 160 2.55 Å for type boscardinite (1.66 Tl *apfu*) could be explained. Consequently, neglecting the
 161 contribution of the (Pb,Tl)₃ site, the ΣTl (in *apfu*) would be 1.04 and 1.36 according to the
 162 bond-valence parameter of Brese and O’Keeffe (1991) and Biagioni *et al.* (2014a),
 163 respectively. This would confirm that the use of the $R_{Tl,S}$ bond-valence parameter by Brese
 164 and O’Keeffe (1991) for mixed (Tl,Pb) results in an overestimation of Pb, as discussed by
 165 Biagioni *et al.* (2015) for chabournéite and protochabournéite.

166 The other sites occurring in the dufrénoysite and sartorite type layers do not show
 167 significant changes in their coordination environments; the only difference is related to the
 168 shortest average $\langle Me-S \rangle$ distances in mixed (Sb/As) sites resulting from the strong
 169 enrichment in As of the studied crystal. Finally, the difference between the average bond

170 distance at the Sb9a position (see Table 6) has to be related to the cut-off distance used for
 171 such a calculation; indeed, by using only $\langle Me^{3+}-S \rangle$ distances shorter than 3.0 Å, Sb at the
 172 Sb9a is bonded to 4 S atoms in type boscardinite (the fifth being at 3.02 Å), whereas in
 173 (Tl,As)-enriched boscardinite there are five S closer than 3.0 Å to Sb9a (the fifth at 2.98 Å).
 174 Considering only the four shortest distances, the average $\langle Sb9a-S \rangle$ distances are 2.646 Å in
 175 both the crystal structures.

176

177 *Polymerization of (Sb,As) sites*

178 Within the sartorite and dufrénoysite type layers, the examination of the shortest (= the
 179 strongest, *i.e.* distance < 2.70 Å, following the approach of Moëlo *et al.*, 2012) $Me^{3+}-S$ bonds
 180 allows the description of the organization of Me^{3+} sites into finite $Me^{3+}_m S_n$ chain fragments
 181 ('polymers' hereafter). By using such a cut-off distance, Sb and As atoms usually show the
 182 classic triangular pyramidal coordination. The exception is represented by the central part of
 183 the dufrénoysite layer with split (Sb/Ag) and (Sb/Pb) positions, having only two short
 184 distances (Sb7) or a single one (Sb10a). Such exceptions are related to uncertainties in these
 185 mixed and split positions.

186 The sartorite layer is characterized by a central 'polymer' $[Sb_4(As_{0.87}Sb_{0.13})_2]_{\Sigma 6} S_{10}$,
 187 with two lateral $(As_{0.60}Sb_{0.40})S_3$ groups (Fig. 2). In type boscardinite, the lateral groups are Sb-
 188 dominant, *i.e.* $(Sb_{0.71}As_{0.29})S_3$. Such a polymeric organization has also been described in the
 189 other thallium-lead sulfosalts from Monte Arsiccio, protochabournéite (Orlandi *et al.*, 2013),
 190 with the 'polymer' $[Sb_4(Sb,As)_2]_{\Sigma 6} S_{10}$ flanked by two isolated $(Sb,As)S_3$ pyramidal groups.
 191 The same configuration occurs in chabournéite from Jas Roux (Biagioni *et al.*, 2015), but the
 192 higher $As/(As+Sb)_{at.}$ ratio with respect to protochabournéite favours the As-to-Sb substitution
 193 at the isolated trigonal pyramids, as observed in (Tl,As)-enriched boscardinite with respect to
 194 type boscardinite, or to possible mean positions (Sb10a – see below).

195 In the dufrénoysite layer, the size of the polymer is determined by the presence or
 196 absence of Sb at the mixed split (Sb/Pb)9 and (Sb/Ag)10 positions. The same configuration
 197 has been reported in other lead sulfosalts: senandorite (Sawada *et al.*, 1987), sartorite
 198 (Berlepsch *et al.*, 2003), the pair sterryite-parasterryite (Moëlo *et al.*, 2012), and carducciite
 199 (Biagioni *et al.*, 2014c).

200 Figure 3 represents the most probable polymerization scheme in the dufrénoysite
 201 layer, according to the following choices:

- 202 i) due to its very low s.o.f. (0.04), Pb9b has been neglected;
- 203 ii) a half occupancy of Ag and Sb on the (Sb/Ag)10 position has been assumed. For
 204 local valence equilibrium, when Ag is present on one position, Sb is present on the
 205 neighbouring equivalent position;
- 206 iii) Sb10a has only one $Me-S$ distance (with S10) shorter than 2.70 Å; however, there
 207 are other three distances only a little longer, ranging between 2.72 and 2.75 Å (a second bond
 208 with S10, and two other bonds with S5 and S6). This Sb10a position is clearly a mean
 209 position between two sub-positions (not represented in Fig. 3), Sb10a' bound to S5 and the
 210 two S10, and Sb10a'' bound to S6 and also to the two S10.

211 On this basis, one obtains the combination of two polymers, $Sb_3(Sb,As)_2(As,Sb)S_{11}$
 212 and $Sb_2(Sb,As)_2(As,Sb)S_9$.

213 Within a dufrénoysite layer, polymers of adjacent identical ribbons (R1 and R2) along
 214 **a** are also connected through (As,Sb)₅ (R1) and Sb_{9a} (R2) via S14 (R1). Moreover, when
 215 present, interlayer Sb_{3b} and Sb_{4b} (Figs. 2 and 3) constitute bridging cations between the
 216 polymers of the two layer types. The resulting polymerization within the whole structure is
 217 thus more complex and variable.

218

219 Discussion

220 Structural formula of (Tl,As)-enriched boscardinite

221 The formula of the (Tl,As)-enriched boscardinite obtained through the crystal structure
 222 refinement is $\text{Ag}_{0.40}\text{Tl}_{1.51}\text{Pb}_{2.10}(\text{Sb}_{7.13}\text{As}_{2.86})_{\Sigma 9.99}\text{S}_{18}$ ($Z = 2$), with the relative error on the
 223 valence equilibrium $E_V(\%) = +0.22$. With respect to the chemical analysis, the $\text{As}/(\text{As}+\text{Sb})_{\text{at}}$
 224 ratio is slightly smaller, *i.e.* 0.29 vs 0.31.

225 This structural formula can be reduced to a stoichiometric one by considering the
 226 structural fragment where the mixed or split sites having different valence states are located
 227 (see Fig. 9 in Orlandi *et al.*, 2012). The composition resulting from these sites is
 228 $\text{Ag}_{0.40}\text{Tl}_{1.51}\text{Pb}_{2.10}\text{Sb}_{1.99}$, and the total valence is 12.08, ideally 12. The sites on the zig-zag
 229 layers correspond to $\text{Tl}_{1.51}\text{Pb}_{2.06}$, which can be simplified as $\text{Tl}_{1.5}\text{Pb}_2$. The two split (Sb,Pb)
 230 and (Sb,Ag) sites correspond to $\text{Ag}_{0.40}\text{Sb}_{1.56}\text{Pb}_{0.04}$. Through the substitution $\text{Ag}^+ + \text{Sb}^{3+} =$
 231 2Pb^{2+} , it becomes $\text{Sb}_{1.16}\text{Pb}_{0.84}$, which can be simplified as SbPb. Thus, the simplified Ag-free
 232 formula of (Tl,As)-enriched boscardinite is $\text{Tl}_{1.5}\text{Pb}_3(\text{Sb}_{6.5}\text{As}_3)_{\Sigma 9.5}\text{S}_{18}$.

233 Nevertheless, it should be emphasized that Ag is always a minor component in
 234 boscardinite. Thus, the composition of the two split (Sb/Pb) and (Sb/Ag) sites could
 235 alternatively be simplified as $\text{Ag}_{0.5}\text{Sb}_{1.5}$. If so, the simplified formula of (Tl,As)-enriched
 236 boscardinite could be $\text{Ag}_{0.5}\text{Tl}_{1.5}\text{Pb}_2(\text{Sb}_7\text{As}_3)_{\Sigma 10}\text{S}_{18}$ ($Z = 2$). Thus, in order to enhance the
 237 possible specific crystal chemical role of Ag, the stoichiometric formula
 238 $\text{AgTl}_3\text{Pb}_4(\text{Sb}_{14}\text{As}_6)_{\Sigma 20}\text{S}_{36}$ ($Z = 1$) would be more convenient. Applying the same consideration
 239 to type boscardinite, the Ag-rich derived formula $\text{AgTl}_2\text{Pb}_6(\text{Sb}_{15}\text{As}_4)_{\Sigma 19}\text{S}_{36}$ is obtained.

240 On the basis of the generalized formula proposed by Orlandi *et al.* (2012),
 241 $\text{Ag}_x\text{Tl}_{1+y}\text{Pb}_{4-2x-2y}(\text{Sb}_{7+x+y+z}\text{As}_{2-z})_{\Sigma 9+x+y}\text{S}_{18}$, (Tl,As)-enriched boscardinite (sample #408) has $x \approx$
 242 0.40, $y \approx 0.50$, and $z \approx -0.90$. Sample #2 corresponds to $x \approx 0.35$, $y \approx 0.40$, and $z \approx -0.80$.

243 (Tl,As)-enriched boscardinite shows a low amount of Hg. This feature agrees with the
 244 Hg-rich nature of the sulfosalt assemblages from Monte Arsiccio (Biagioni *et al.*, 2013) and
 245 the association of samples #408 and #2 with routhierite, $\text{CuHg}_2\text{TlAs}_2\text{S}_6$, and cinnabar, HgS,
 246 respectively. Hg could be hosted at the partially occupied Ag10b site, in agreement with the
 247 Hg^{2+} to Ag^+ substitution observed in other lead sulfosalts (*e.g.*, rouxelite – Orlandi *et al.*,
 248 2005; Biagioni *et al.*, 2014b).

249

250 Comparison with type boscardinite

251 As stated in the introduction, these new occurrences of boscardinite are definitely
 252 enriched in As (as well as Tl) with respect to the type specimen. The $\text{As}/(\text{As}+\text{Sb})_{\text{at}}$ ratio is
 253 0.31 (sample #408), to be compared with 0.21-0.24 of type specimen. This explains the
 254 volume decrease of (Tl,As)-enriched boscardinite ($\approx -0.8\%$). Nevertheless, while the *b*
 255 parameter decreases (-1.15%), *a* and *c* slightly increase (0.11 and 0.27%, respectively).

256 Indeed, two competing mechanisms take place: a volume decrease, related to the As-Sb
257 substitution, and a volume increase due to the Tl-Pb replacement.

258 In the crystal structure of (Tl,As)-enriched boscardinite, As exceeds Sb in three sites:
259 As₃, As₄, and As₈. Sb₅ has a s.o.f. close to Sb_{0.5}As_{0.5}. In type boscardinite, only one site
260 (As₄) is an As-dominant site. The main As-enrichment is observed in the sartorite type layer
261 relatively to the dufrénoysite type one. In the former layer, the As/(As+Sb)_{at.} ratio is 0.368, to
262 be compared with 0.26 in type boscardinite. In the latter, the ratio is 0.250, to be compared
263 with 0.125 in type specimen. The predominantly As- and Sb-occupied sites are distributed
264 within the layers in a chess-board pattern (Fig. 3), similar to those observed in other members
265 of the sartorite homologous series (*e.g.*, guettardite – Makovicky *et al.*, 2012; twinnite –
266 Makovicky and Topa, 2012; barikaite – Makovicky and Topa, 2013). This As-versus-Sb
267 partitioning appears as the main factor controlling the ~8 Å superstructure, that permits to
268 minimize the steric distortions between As- and Sb-rich sites.

269 Tl-rich sites are closely bound to the polymeric organization of (Sb/As) sites of the
270 sartorite type layer, *i.e.* of the As-rich layer; the reverse is true for Pb-rich sites which are
271 preferentially bound to the dufrénoysite type layer. On this basis, the structural formula can be
272 cut into two sub-parts (formula refers to ribbons):

273 (1) sartorite-type layer, with Tl-rich sites: $[(\text{Tl}_{3.02}\text{Pb}_{0.98})_{\Sigma 4}(\text{Sb}_{5.06}\text{As}_{2.94})_{\Sigma 8}\text{S}_{16}]^{-3.02}$;
274 (2) dufrénoysite-type layer, with Pb-rich sites:
275 $[(\text{Pb}_{3.136}\text{Sb}_{0.864})_{\Sigma 4}(\text{Ag}_{0.80}\text{Pb}_{0.088}\text{Sb}_{8.332}\text{As}_{2.78})_{\Sigma 12}\text{S}_{20}]^{+3.18}$.

276 Contrary to type boscardinite, this new occurrence displays Pb-rich sites containing
277 some Sb, without any Tl (even if Tl at the Pb₃ site in type boscardinite could be due to a
278 misinterpretation – see above).

279

280 *(Tl,As)-enriched boscardinite: variety or a new mineral species?*

281 Boscardinite, ideally $\text{TlPb}_4(\text{Sb}_7\text{As}_2)_{\Sigma 9}\text{S}_{18}$, and (Tl,As)-enriched boscardinite, ideally
282 $\text{Tl}_{1.5}\text{Pb}_3(\text{Sb}_{6.5}\text{As}_3)_{\Sigma 9.5}\text{S}_{18}$, significantly differ both chemically and structurally. Clearly, these
283 differences are remarkable from a crystal-chemical point of view, giving new insights on the
284 As-to-Sb partitioning in the members of the sartorite homologous series. Nevertheless, these
285 differences are not sufficient to propose a new mineral species.

286 Two kinds of substitution take place: (1) the isovalent $\text{Sb}^{3+} = \text{As}^{3+}$ substitution, and (2)
287 the heterovalent $\text{Tl}^+ + \text{Me}^{3+} = 2\text{Pb}^{2+}$. Substitution (1) involves the occurrence of sites having
288 different As- or Sb-dominance, but with $\text{As}_{\text{tot}} < \text{Sb}_{\text{tot}}$ as in type boscardinite. In boscardinite
289 and its (Tl,As)-enriched analogue, the As-to-Sb substitution does not cause any different
290 crystallographic characteristic between the two phases, *i.e.* no different symmetries, or space
291 groups, or superstructures. Substitution (2): taking into account the Tl substitution percentage,
292 boscardinite and its (Tl,As)-enriched isotype are intermediate members between the
293 unsubstituted $\text{Pb}_6(\text{Sb,As})_8\text{S}_{18}$ and the fully substituted Tl endmember $\text{Tl}_3(\text{Sb,As})_{11}\text{S}_{18}$. The Tl
294 subst. % values, calculated following the procedure described by Makovicky and Topa (2015)
295 range from ~ 37% (sample #4989 of type boscardinite) and ~ 50% of sample #408 of (Tl,As)-
296 enriched boscardinite. As stressed in the previous paragraph, Ag seems to be a minor but
297 characteristic component of boscardinite. The Ag subst. % values range between ~30%
298 (sample #4989) and 43% (sample #408).

299 From these calculations, it appears that (Tl,As)-enriched boscardinite does not
 300 significantly exceed the 50% substitution neither of Tl nor Ag (and obviously of As) and
 301 consequently it should be considered only as a (Tl,As)-enriched variety of boscardinite.
 302 Actually, sample #408 has a Tl subst. % slightly higher than 50 (*i.e.*, 50.33%). But it should
 303 be taken in mind that, even if the experimental error is neglected, the known compositional
 304 range of boscardinite ranges between 30 and 50%. Thus, the rule proposed by Nickel (1992)
 305 could be applied: “*If the known compositions embrace the 50% mark but do not appear to*
 306 *extend to either end-member [...], only one name should be applied to the compositional*
 307 *range*”. In conclusion, (Tl,As)-enriched boscardinite can be simply considered as a variety of
 308 boscardinite.

309

310 *What is the exact definition of boscardinite?*

311 Initially, members of the sartorite homologous series were defined as lead-arsenic
 312 sulfosalts. Later, since the first description of antimonian baumhauerite from Madoc, Ontario,
 313 Canada (Jambor, 1967a, 1967b), Sb-containing analogues were described. Boscardinite was
 314 the first $N = 3.5$ homologue having $Sb > As$. Actually, it is the Tl-Sb analogue of
 315 baumhauerite, ideally $Pb_6As_8S_{18}$. Recently, a new $N = 3.5$ homologues characterized by the
 316 occurrence of Sb and As has been described: bernarlottiite, $Pb_6(As_5Sb_3)S_{18}$ (Orlandi *et al.*,
 317 2014).

318 Type boscardinite was defined as $TlPb_4(Sb_7As_2)_{\Sigma 9}S_{18}$. Its chemical variability points to
 319 even higher Tl and As contents, up to $Tl_{1.5}Pb_3(Sb_{6.5}As_3)_{\Sigma 9.5}S_{18}$. Increasing the Tl content, one
 320 could obtain the compound $Tl_2Pb_2(Sb,As)_{10}S_{18}$, *i.e.* $TlPb(Sb,As)_5S_9$. This chemical formula
 321 corresponds to the Sb analogue of hutchinsonite, $TlPbAs_5S_9$, a mineral showing a different
 322 structural arrangement, belonging to the hutchinsonite merotypic series (Makovicky, 1997).
 323 Actually, the role of Ag in the $N = 3.5$ homologue structure is not known; it could
 324 hypothetically stabilize boscardinite up to higher Tl content. Ag content similar to those
 325 occurring in boscardinite seems to control the formation and to give rise to superstructure
 326 reflections in “baumhauerite-2a” (Laroussi *et al.*, 1989; Pring *et al.*, 1990; Pring and Graeser,
 327 1994), recently redefined as argentobaumhauerite (Hålenius *et al.*, 2015). On the contrary,
 328 type boscardinite, studied using synchrotron radiation, does not show superstructure
 329 reflections. However, the hypothesis of the possible existence of domains of “boscardinite-
 330 2a” within a boscardinite matrix could not be discarded. Further study will be mandatory.

331 The comparison of boscardinite with other members of the sartorite homologous series
 332 is interesting. If two unit formulas of sartorite, ideally $PbAs_2S_4$, are added to two units of the
 333 ideal formula of philrothite, $TlAs_3S_5$ (Bindi *et al.*, 2014), one gets:



335 corresponding to an As-analogue of (Tl,As)-enriched boscardinite, with one Pb replaced by
 336 $(0.5Tl + 0.5As)$.

337 Boscardinite is currently defined as the Tl-Sb analogue of baumhauerite, with
 338 idealized formula $Tl_{1+x}Pb_{4-2x}(Sb,As)_{9+x}S_{18}$ ($0 < x < 0.5$). If $x < 0$, then a new potential Sb-
 339 baumhauerite is obtained. Tl contents higher than 1.5 *apfu* ($x > 0.5$) should enlarge the
 340 compositional field of boscardinite, potentially leading to a new chemical pole.

341

342 *Thallium-lead sulfosalts from the Monte Arsiccio mine*

343 Boscardinite, as well as protochabournéite, are the two thallium-lead sulfosalts having
 344 their type locality at the Monte Arsiccio mine, Apuan Alps, Tuscany, Italy. This small baryte
 345 + pyrite + iron oxides abandoned mine has recently become a reference locality for the study
 346 of thallium sulfosalts. In addition to thallium sulfosalts *sensu stricto*, Tl-bearing varieties of
 347 rouxelite, robinsonite, chovanite, and twinnite have been identified (*e.g.*, Biagioni *et al.*,
 348 2014b). Three kinds of sulfosalt occurrences have been identified:

- 349 i) Type 1: microcrystalline baryte + pyrite ore bodies, at the contact between schists
 350 and dolostones;
 351 ii) Type 2: pyrite-rich dolostones, near the contact with the schists;
 352 iii) Type 3: carbonate (usually dolomite) ± baryte ± quartz veins embedded in the
 353 dolostones.

354 The complexity of the ore geochemistry at Monte Arsiccio and these different kinds of
 355 sulfosalt occurrences are reflected in the crystal-chemistry of the studied minerals. Biagioni *et*
 356 *al.* (2014a) discussed the chemical variability of the pair arsiccioite-routhierite as a function
 357 of their kind of occurrence, showing an increase in the $As/(As+Sb)_{at.}$ ratio passing from the
 358 pyrite-rich dolostone to the microcrystalline baryte + pyrite ore bodies.

359 New chemical data collected on boscardinite and protochabournéite seem to confirm
 360 such a significant chemical variability in sulfosalts. Figure 4 shows the $Pb/(Pb+2Tl)$ *versus*
 361 $As/(As+Sb)$ atomic ratio in the chabournéite series and boscardinite. In addition to the two
 362 new chemical analyses of boscardinite reported above, other three samples were chemically
 363 characterized previously, representative of Type 2 and Type 1 occurrences (unpublished data).
 364 Two additional samples from Type 2 occurrence (#371 and #409) have chemical composition
 365 (on the basis of $\Sigma Me = 14$ *apfu*) $Ag_{0.40}Tl_{1.20}Pb_{2.75}Hg_{0.01}(Sb_{7.00}As_{2.64})_{\Sigma 9.64}S_{18.20}$ and
 366 $Ag_{0.34}Tl_{1.35}Pb_{2.59}Hg_{0.02}(Sb_{6.88}As_{2.81})_{\Sigma 9.69}S_{18.24}$, with $As/(As+Sb)_{at.}$ ratio of 0.274 and 0.290,
 367 respectively. Boscardinite from Type 1 occurrence (sample #404) is richer in As than sample
 368 #408, having chemical composition $Ag_{0.38}Tl_{1.42}Pb_{2.45}Hg_{0.02}(Sb_{6.52}As_{3.21})_{\Sigma 9.73}S_{18.18}$, with
 369 $As/(As+Sb)_{at.}$ ratio of 0.330. Consequently, boscardinite seems to show an increase in Tl and
 370 As passing from Type 3 occurrence (Type boscardinite, TB in Figure 4) to Type 1 occurrence
 371 (sample #404). In addition, (Tl,As)-enriched boscardinite has been identified in the Sant'Anna
 372 level, in association with a “protochabournéite-like” mineral. It is interesting to observe that
 373 the $Pb/(Pb+2Tl)_{at.}$ ratio of (Tl,As)-enriched boscardinite is similar to the “Pb-excess
 374 chabournéite derivative” reported from Abuta, Japan, by Johan *et al.* (1981). Owing to the
 375 absence of structural data on this latter compound, its relationships with boscardinite are not
 376 known but it could also correspond to an “As-rich derivative of boscardinite”.

377 Protochabournéite, originally described from Type 2 and 3 occurrences, was later
 378 identified in Type 1 occurrence (sample C02 in Figure 2). Its chemical analysis gave the
 379 following result [same analytical conditions described for (Tl,As)-enriched boscardinite] (in
 380 wt%, mean of 4 spot analyses): Tl 18.06(11), Pb 8.81(13), Sb 41.93(53), As 6.73(18), S
 381 23.57(19), sum 99.10(96). Its chemical formula, on the basis of $\Sigma Me = 13$ *apfu*, is
 382 $Tl_{2.03(1)}Pb_{0.98(1)}Sb_{7.92(4)}As_{2.07(5)}S_{16.91(7)}$, $Ev(\%) = +0.4$. This new occurrence is similar to
 383 analysis of sample A in Orlandi *et al.* (2013), with a slightly higher Tl content. On the
 384 contrary, the “protochabournéite-like” mineral observed intimately associated with (Tl,As)-
 385 enriched boscardinite from the Sant'Anna level has some chemical peculiarities, showing
 386 high $Pb/(Pb+2Tl)$ and $As/(As+Sb)_{at.}$ ratios with respect to type protochabournéite. Its

387 chemical analyses (average of 3 spot analyses) gave (in wt%): Tl 15.85(6), Pb 13.52(43), Hg
388 0.04(3), Sb 38.84(22), As 7.76(22), S 23.70(25), Cl 0.05(1), sum 99.77(113). The chemical
389 formula is $\text{Tl}_{1.78(2)}\text{Pb}_{1.50(3)}\text{Hg}_{0.01(1)}\text{Sb}_{7.33(5)}\text{As}_{2.38(4)}\text{S}_{16.99(6)}\text{Cl}_{0.03(1)}$, $E_V(\%) = -0.2$. An X-ray
390 diffraction study is necessary to confirm its identity with protochabournéite.

391

392 **Conclusion**

393 The thallium-rich sulfosalt assemblage from Monte Arsiccio represents an interesting
394 field of research for the study of sulfosalt crystal-chemistry owing to its complex
395 geochemistry, associating Tl with Pb, Sb, As, Ag, Hg, and Cu. The occurrence of a (Tl,As)-
396 rich variety of boscardinite refines the knowledge about the $N = 3.5$ homologues of the
397 sartorite series, providing new data on the partitioning of As and Sb within these compounds.
398 The upper limit in Tl content in $N = 3.5$ homologues, as well as the role of Ag, should be
399 clarified by further studies.

400 The chemical variability observed in thallium-lead sulfosalts confirms the exceptional
401 mineralogical complexity of the baryte-pyrite-iron oxides ore deposits from the Apuan Alps,
402 where small changes in the ore geochemistry control the crystallization of a great variety of
403 different sulfosalts.

404

405 **Acknowledgements**

406 Electron microprobe analyses were performed with the help of J. Langlade (engineer,
407 “Microsonde Ouest” laboratory, IFREMER, Plouzané, France). This research received
408 support by MIUR through project SIR 2014 “THALMIGEN – Thallium: Mineralogy,
409 Geochemistry, and Environmental Hazards”, granted to CB. The manuscript benefited of the
410 comments of Emil Makovicky and an anonymous reviewer.

411

412 **REFERENCES**

- 413 Berlepsch, P., Armbruster, T. and Topa, D. (2002) Structural and chemical variations in
 414 rathite, $Pb_8Pb_{4-x}(Tl_2As_2)_x(Ag_2As_2)As_{16}S_{40}$: modulations of a parent structure. *Zeitschrift*
 415 *für Mineralogie*, **217**, 581–590.
- 416 Berlepsch, P., Armbruster, T., Makovicky, E. and Topa, D. (2003) Another step toward
 417 understanding the true nature of sartorite: determination and refinement of a ninefold
 418 superstructure. *American Mineralogist*, **88**, 450–461.
- 419 Biagioni, C., D’Orazio, M., Vezzoni, S., Dini, A. and Orlandi, P. (2013) Mobilization of Tl-
 420 Hg-As-Sb-(Ag,Cu)-Pb sulfosalt melts during low-grade metamorphism in the Alpi
 421 Apuane (Tuscany, Italy). *Geology*, **41**, 747–751.
- 422 Biagioni, C., Bonaccorsi, E., Moëlo, Y., Orlandi, P., Bindi, L., D’Orazio, M. and Vezzoni, S.
 423 (2014a) Mercury-arsenic sulfosalts from the Apuan Alps (Tuscany, Italy). II.
 424 Arsiccioite, $AgHg_2TlAs_2S_6$, a new mineral from the Monte Arsiccio mine: occurrence,
 425 crystal structure and crystal chemistry of the routhierite isotopic series. *Mineralogical*
 426 *Magazine*, **78**, 101–117.
- 427 Biagioni, C., Moëlo, Y. and Orlandi, P. (2014b) Lead-antimony sulfosalts from Tuscany
 428 (Italy). XV. (Tl-Ag)-bearing rouxelite from Monte Arsiccio mine: occurrence and
 429 crystal structure. *Mineralogical Magazine*, **78**, 651–661.
- 430 Biagioni, C., Orlandi, P., Moëlo, Y. and Bindi, L. (2014c) Lead-antimony sulfosalts from
 431 Tuscany (Italy). XVI. Carducciite, $(AgSb)Pb_6(As,Sb)_8S_{20}$, a new Sb-rich derivative of
 432 rathite from the Pollone mine, Valdicastello Carducci: occurrence and crystal structure.
 433 *Mineralogical Magazine*, **78**, 1775–1793.
- 434 Biagioni, C., Moëlo, Y., Favreau, G., Bourgoin, V. and Boulliard, J.-C. (2015) Structure of
 435 Pb-rich chabournéite from Jas Roux, France. *Acta Crystallographica*, **B71**, 81–88.
- 436 Bindi, L., Nestola, F., Makovicky, E., Guastoni, A. and De Battisti, L. (2014) Tl-bearing
 437 sulfosalt from the Lengenbach quarry, Binn Valley, Switzerland: Philrothite, $TlAs_3S_5$.
 438 *Mineralogical Magazine*, **78**, 1–9.
- 439 Brese, N.E. and O’Keeffe, M. (1991) Bond-valence parameters for solids. *Acta*
 440 *Crystallographica*, **B47**, 192–197.
- 441 Bruker AXS Inc. (2004) APEX 2. Bruker Advanced X-ray Solutions, Madison, Wisconsin,
 442 USA.
- 443 Hålenius, U., Hatert, F., Pasero, M. and Mills, S.J. (2015) IMA Commission on New
 444 Minerals, Nomenclature and Classification (CNMNC) Newsletter 25. *Mineralogical*
 445 *Magazine*, **79**, 529–535.
- 446 Jambor, J.L. (1967a) New lead sulfantimonides from Madoc, Ontario – Part 1. *The Canadian*
 447 *Mineralogist*, **9**, 7 – 24.
- 448 Jambor, J.L. (1967b) New lead sulfantimonides from Madoc, Ontario. Part 2 – Mineral
 449 descriptions. *The Canadian Mineralogist*, **9**, 191–213.
- 450 Johan, Z., Mantiene, J. and Picot, P. (1981) La chabournéite, un nouveau minéral thallifère.
 451 *Bulletin de Minéralogie*, **104**, 10–15.
- 452 Laroussi, A., Moëlo, Y., Ohnenstetter, D. and Ginderow, D. (1989) Argent et thallium dans
 453 les sulfosels de la série de la sartorite (gisement de Lengenbach, vallée de Binn, Suisse).
 454 *Comptes Rendus de l’Académie des Sciences Paris*, **308**, 927–933.

- 455 Makovicky, E. (1985) The building principles and classification of sulphosalts based on the
456 SnS archetype. *Fortschritte der Mineralogie*, **63**, 45–89.
- 457 Makovicky, E. (1997) Modular crystal chemistry of sulphosalts and other complex sulphides.
458 *In Modular Aspects of Minerals* (S. Merlino, ed.). *European Mineralogical Union*,
459 *Notes in Mineralogy*, **1**, 237–271.
- 460 Makovicky, E. and Topa, D. (2012) Twinnite, $Pb_{0.8}Tl_{0.1}Sb_{1.3}As_{0.8}S_4$, the OD character and the
461 question of its polytypism. *Zeitschrift für Kristallographie*, **227**, 468–475.
- 462 Makovicky, E. and Topa, D. (2013) The crystal structure of barikaite. *Mineralogical*
463 *Magazine*, **77**, 3093–3104.
- 464 Makovicky, E. and Topa, D. (2015) Crystal chemical formula for sartorite homologues.
465 *Mineralogical Magazine*, **79**, 25–31.
- 466 Makovicky, E., Topa, D., Tajjedin, H., Rastad, E. and Yaghubpur, A. (2012) The crystal
467 structure of guettardite, $PbAsSbS_4$, and the twinnite-guettardite problem. *The Canadian*
468 *Mineralogist*, **50**, 253–265.
- 469 Mantiene, J. (1974) La minéralisation thallifère de Jas Roux (Hautes-Alpes). Unpublished
470 thesis, Université de Paris, 146 p.
- 471 Moëlo, Y., Guillot-Deudon, C., Evain, M., Orlandi, P. and Biagioni, C. (2012) Comparative
472 modular analysis of two complex sulfosalts structures: sterryite,
473 $Cu(Ag,Cu)_3Pb_{19}(Sb,As)_{22}(As-As)S_{56}$, and parasterryite, $Ag_4Pb_{20}(Sb,As)_{24}S_{58}$. *Acta*
474 *Crystallographica*, **B68**, 480–492.
- 475 Nestola, F., Guastoni, A., Bindi, L. and Secco, L. (2009) Dalnegroite, $Tl_{5-x}Pb_{2x}(As,Sb)_{21-x}S_{34}$,
476 a new thallium sulphosalt from Lengenbach quarry, Binntal, Switzerland. *Mineralogical*
477 *Magazine*, **73**, 1027–1032.
- 478 Nickel, E.H. (1992) Nomenclature for mineral solid solutions. *American Mineralogist*, **77**,
479 660–662.
- 480 Orlandi, P., Moëlo, Y., Meerschaut, A., Palvadeau, P. and Léone, P. (2005) Lead-antimony
481 sulfosalts from Tuscany (Italy). VIII. Rouxelite, $Cu_2HgPb_{22}Sb_{28}S_{64}(O,S)_2$, a new
482 sulfosalt from Buca della Vena mine, Apuan Alps: definition and crystal structure. *The*
483 *Canadian Mineralogist*, **43**, 919–933.
- 484 Orlandi, P., Biagioni, C., Bonaccorsi, E., Moëlo, Y. and Paar, W. (2012) Lead-antimony
485 sulfosalts from Tuscany (Italy). XII. Boscardinite, $TlPb_4(Sb_7As_2)_{\Sigma 9}S_{18}$, a new mineral
486 species from the Monte Arsiccio mine: occurrence and crystal structure. *The Canadian*
487 *Mineralogist*, **50**, 235–251.
- 488 Orlandi, P., Biagioni, C., Moëlo, Y., Bonaccorsi, E. and Paar, W. (2013) Lead-antimony
489 sulfosalts from Tuscany (Italy). XIII. Protochabournéite, $\sim Tl_2Pb(Sb_{9.8}As_{1.2})_{\Sigma 10}S_{17}$, from
490 the Monte Arsiccio mine: occurrence, crystal structure and relationship with
491 chabournéite. *The Canadian Mineralogist*, **51**, 475–494.
- 492 Orlandi, P., Biagioni, C., Bonaccorsi, E., Moëlo, Y. and Paar, W.H. (2014) Bernarlottiite,
493 IMA 2013-133. CNMNC Newsletter No. 20, June 2014, page 553. *Mineralogical*
494 *Magazine*, **78**, 549–558.
- 495 Pring, A. and Graeser, S. (1994) Polytypism in baumhauerite. *American Mineralogist*, **79**,
496 302–307.

- 497 Pring, A., Birch, W.D., Sewell, D., Graeser, S., Edenharter, A. and Criddle, A. (1990)
498 Baumhauerite-2a: A silver-bearing mineral with a baumhauerite-like supercell from
499 Lengenbach, Switzerland. *American Mineralogist*, **75**, 915–922.
- 500 Sawada, H., Kawada, I., Hellner, E. and Tokonami, M. (1987) The crystal structure of
501 senandorite (andorite VI): $\text{PbAgSb}_3\text{S}_6$. *Zeitschrift für Kristallographie*, **180**, 141–150.
- 502 Sheldrick, G.M. (2008) A short history of SHELX. *Acta Crystallographica*, **A64**, 112–122.
- 503 Shimizu, M., Matsuyama, F. and Shimizu, M. (1999) Hutchinsonite, $\text{TlPb}(\text{As,Sb})_5\text{S}_9$,
504 Chabournéite, $\text{Tl}_2\text{Pb}(\text{Sb,As})_{10}\text{S}_{17}$, and Unnamed $(\text{Tl,Ag})_2\text{Pb}_6(\text{As,Sb})_{16}\text{S}_{31}$ from the
505 Toya-Takarada Mine, Hokkaido, Japan – Tl mineralisation in the Kuroko Deposits.
506 *Resource Geology*, **20**, 31–37.
- 507 Topa, D., Makovicky, E., Favreau, G., Bourgoïn, V., Boulliard, J.-C., Zagler, G. and Putz,
508 H. (2013) Jasrouxite, a new Pb-Ag-As-Sb member of the lillianite homologous series
509 from Jas Roux, Hautes-Alpes, France. *European Journal of Mineralogy*, **25**, 1031–
510 1038.
- 511 Wilson, A.J.C. (1992) International Tables for X-ray Crystallography Volume C. Kluwer,
512 Dordrecht.
513

514 **Table captions**

515 **Table 1.** Microprobe analyses of (Tl,As)-enriched boscardinite: chemical composition as wt%
516 and chemical formula (in atoms per formula unit, *apfu*) on the basis of $\Sigma Me = 14$ *apfu*.

517 **Table 2.** Crystal data and summary of parameters describing data collection and refinement
518 for (Tl,As)-enriched boscardinite.

519 **Table 3.** Atomic positions and equivalent displacement parameters (in \AA^2) for (Tl,As)-
520 enriched boscardinite.

521 **Table 4.** Selected bond distances (in \AA) for (Tl,As)-enriched boscardinite.

522 **Table 5.** Bond-valence balance (in valence unit, *vu*) in (Tl,As)-enriched boscardinite using the
523 parameters proposed by Brese and O’Keeffe (1991).

524 **Table 6.** Site occupancies in type boscardinite (Orlandi *et al.*, 2012) and in (Tl,As)-enriched
525 boscardinite. Site labels agree with those given in Table 3. Average $\langle Me-S \rangle$ distances for
526 (Sb/As) sites have been calculated considering bond distances shorter than 3.0 \AA .

527 **Table 7.** Proposed site occupancies at mixed (Tl/Pb) sites. Site occupancies calculated
528 according to the bond-valence parameter $R_{Tl,S}$ proposed by Brese and O’Keeffe (1991) (B &
529 O) and by Biagioni *et al.* (2014a) (B *et al.*).

530

531 **Figure captions**

532 **Figure 1.** Crystal structure of (Tl,As)-rich boscardinite as seen down **b**. Numbers without
533 specification refer to S sites.

534 **Figure 2.** Polymerization within the sartorite layer of (Tl,As)-enriched boscardinite.

535 **Figure 3.** Main polymerization scheme (proposal) within the dufrénoysite layer of (Tl,As)-
536 rich boscardinite (Pb9b absent, Sb10a alternation with Ag10b). Blue lines enclose the two
537 polymers $Sb_3(Sb,As)_2(As,Sb)S_{11}$ and $Sb_2(Sb,As)_2(As,Sb)S_9$. Black arrow: shift of Sb10a
538 towards S6 (a shift towards S5 is equiprobable).

539 **Figure 4** $As/(As+Sb)$ versus $Pb/(Pb+2Tl)$ atomic ratio in the chabournéite series and in
540 boscardinite. Lozenges: chabournéite (data after Mantiene, 1974; Johan *et al.*, 1981; Shimizu
541 *et al.*, 1999; Biagioni *et al.*, 2015; D. Harris, writ. commun., 1989) and dalnegroite (Nestola *et al.*,
542 2009). Triangles: protochabournéite (A and B correspond to analyses given in Orlandi *et al.*,
543 2013). Square: boscardinite (4977 and 4989 correspond to analyses of type boscardinite
544 given in Orlandi *et al.*, 2012; the remaining analyses are discussed in the text). Circles: “Pb-
545 excess chabournéite derivative or As-boscardinite derivative (data after Johan *et al.*, 1981)
546 and ideal chemical composition of hutchinsonite, $TlPbAs_5S_9$.

547

548 **Table 1.** Microprobe analyses of (Tl,As)-enriched boscardinite: chemical composition as wt%
 549 and chemical formula (in atoms per formula unit, *apfu*) on the basis of $\Sigma Me = 14$ *apfu*.
 550

Element	Sant'Olga (sample #408)			Sant'Anna (sample #2)		
	wt%	Range (n = 3)	e.s.d.	wt%	Range (n = 3)	e.s.d.
Ag	1.81	1.77 – 1.87	0.05	1.46	1.42 – 1.51	0.05
Tl	12.60	12.39 – 12.82	0.21	11.38	11.33 – 11.43	0.05
Pb	17.99	17.85 – 18.09	0.12	20.57	20.46 – 20.79	0.19
Hg	0.14	0.10 – 0.20	0.05	0.13	0.10 – 0.16	0.03
As	9.36	9.23 – 9.46	0.12	8.24	8.22 – 8.24	0.01
Sb	33.60	33.28 – 33.77	0.27	33.48	33.39 – 33.55	0.08
S	23.41	23.09 – 23.70	0.30	22.89	22.81 – 22.96	0.07
Cl	0.06	0.05 – 0.07	0.01	0.05	0.03 – 0.08	0.03
sum	98.97	97.82 – 99.56	1.00	98.20	98.15 – 98.27	0.06
<i>apfu</i>						
Ag	0.42	0.40 – 0.43	0.01	0.34	0.33 – 0.35	0.01
Tl	1.52	1.51 – 1.54	0.01	1.41	1.40 – 1.42	0.01
Pb	2.14	2.14 – 2.15	0.01	2.51	2.50 – 2.53	0.02
Hg	0.02	0.01 – 0.02	0.01	0.02	0.01 – 0.02	0.00
As	3.08	3.07 – 3.10	0.01	2.78	2.77 – 2.78	0.00
Sb	6.82	6.81 – 6.83	0.01	6.95	6.94 – 6.97	0.02
S	18.04	17.96 – 18.16	0.11	18.04	17.96 – 18.11	0.08
Cl	0.04	0.04 – 0.05	0.00	0.04	0.02 – 0.06	0.02
Ev (%)*	-0.4	-1.1 – -0.1	0.6	-0.4	-0.9 – 0.1	0.5

551 * Relative error on the valence equilibrium (%), calculated as $[\Sigma(\text{val}+) - \Sigma(\text{val}-)] \times 100 / \Sigma(\text{val}-)$.
 552

553
 554

555 **Table 2.** Crystal data and summary of parameters describing data collection and refinement
 556 for (Tl,As)-enriched boscardinite.
 557

Crystal data	
Structural formula	Ag _{0.40} Tl _{1.51} Pb _{2.10} (Sb _{7.13} As _{2.86}) _{Σ9.99} S ₁₈
Crystal size (mm)	0.10 x 0.10 x 0.05
Cell setting, space group	Triclinic, $P\bar{1}$
<i>a</i> , <i>b</i> , <i>c</i> (Å);	8.1017(4), 8.6597(4), 22.5574(10);
α , β , γ (°)	90.666(2), 97.242(2), 90.850(2)
<i>V</i> (Å ³)	1569.63(12)
<i>Z</i>	2
Data collection and refinement	
Radiation, wavelength (Å)	Mo <i>K</i> α , $\lambda = 0.71073$
Temperature (K)	293
Maximum observed 2θ (°)	55.31
Measured reflections	26678
Unique reflections	7211
Reflections $F_o > 4 \sigma F_o$	6582
R_{int} after absorption correction	0.0195
$R\sigma$	0.0171
Range of <i>h</i> , <i>k</i> , <i>l</i>	$-10 \leq h \leq 10$, $-11 \leq k \leq 11$, $-29 \leq l \leq 29$
$R [F_o > 4 \sigma F_o]$	0.0285
R (all data)	0.0330
wR (on F_o^2)	0.0707
Goof	1.115
Number of least-squares parameters	314
Maximum and minum residual peak (e/Å ³)	2.70 (at 0.73 Å from Pb3a) -3.38 (at 0.67 Å from Sb4b)

558

559

560 **Table 3.** Atomic positions and equivalent displacement parameters (in Å²) for (Tl,As)-
 561 enriched boscardinite.
 562

Site	Occupancy	<i>x/a</i>	<i>y/b</i>	<i>z/c</i>	<i>U</i> _{eq} (Å ²)
Tl1	Tl _{0.90} Pb _{0.10}	0.12401(5)	0.63926(4)	0.17007(1)	0.0407(1)
Tl2a	Tl _{0.23} Pb _{0.18}	0.8661(5)	0.8796(4)	0.8247(2)	0.0446(4)
Tl2b	Tl _{0.38} Pb _{0.21}	0.8339(3)	0.8481(2)	0.8293(1)	0.0446(4)
Pb3a	Pb _{0.757(5)}	0.6717(2)	0.6538(3)	0.2605(1)	0.0423(3)
Sb3b	Sb _{0.243(5)}	0.6977(15)	0.653(2)	0.2589(8)	0.0423(3)
Pb4a	Pb _{0.811(5)}	0.66469(10)	0.14674(11)	0.25837(4)	0.0427(2)
Sb4b	Sb _{0.189(5)}	0.6654(10)	0.1672(9)	0.2435(3)	0.0427(2)
Sb1	Sb _{1.00}	0.55493(6)	0.39577(6)	0.10135(2)	0.0256(1)
Sb2	Sb _{1.00}	0.82275(6)	0.10871(5)	0.01945(2)	0.0231(1)
As3	As _{0.60(1)} Sb _{0.40(1)}	0.46832(8)	0.11462(7)	0.88187(3)	0.0280(2)
As4	As _{0.87(1)} Sb _{0.13(1)}	0.18682(8)	0.36301(8)	0.00280(3)	0.0240(2)
Sb5	Sb _{0.51(1)} As _{0.49(1)}	0.07572(7)	0.39082(7)	0.33278(3)	0.0280(2)
Sb6	Sb _{0.73(1)} As _{0.27(1)}	0.11230(7)	0.85087(7)	0.34549(2)	0.0312(2)
Sb7	Sb _{1.00}	0.84624(6)	0.34108(6)	0.46601(2)	0.0327(1)
As8	As _{0.63(1)} Sb _{0.37(1)}	0.79017(8)	0.90055(8)	0.44478(3)	0.0344(2)
Sb9a	Sb _{0.956(3)}	0.43016(14)	0.15697(12)	0.41082(3)	0.0327(2)
Pb9b	Pb _{0.044(3)}	0.382(2)	0.1197(14)	0.4157(5)	0.0327(2)
Sb10a	Sb _{0.60(1)}	0.4774(4)	0.6011(4)	0.4285(2)	0.0472(6)
Ag10b	Ag _{0.40(1)}	0.4708(7)	0.6340(6)	0.4138(3)	0.0472(6)
S1	S _{1.00}	0.3622(2)	0.1791(2)	0.04453(10)	0.0336(4)
S2	S _{1.00}	0.9243(2)	0.6928(2)	0.39903(9)	0.0286(4)
S3	S _{1.00}	0.2737(2)	0.9117(2)	0.85895(7)	0.0235(3)
S4	S _{1.00}	0.9092(2)	0.3927(2)	0.23876(9)	0.0342(4)
S5	S _{1.00}	0.6267(2)	0.3579(2)	0.37759(8)	0.0261(3)
S6	S _{1.00}	0.6707(2)	0.1684(2)	0.51583(8)	0.0270(4)
S7	S _{1.00}	0.9918(2)	0.0921(2)	0.93289(7)	0.0212(3)
S8	S _{1.00}	0.9297(2)	0.8801(2)	0.25565(8)	0.0273(4)
S9	S _{1.00}	0.3328(2)	0.5684(2)	0.05246(8)	0.0247(3)
S10	S _{1.00}	0.2959(2)	0.4240(2)	0.47268(10)	0.0322(4)
S11	S _{1.00}	0.9699(3)	0.0885(2)	0.41704(11)	0.0377(5)
S12	S _{1.00}	0.9850(2)	0.3412(2)	0.06757(8)	0.0241(3)
S13	S _{1.00}	0.5736(2)	0.9272(3)	0.36456(9)	0.0359(4)
S14	S _{1.00}	0.2555(2)	0.1942(2)	0.30754(8)	0.0314(4)
S15	S _{1.00}	0.7096(2)	0.6768(2)	0.14139(8)	0.0249(3)
S16	S _{1.00}	0.2547(2)	0.6023(2)	0.31409(9)	0.0299(4)
S17	S _{1.00}	0.4410(2)	0.3767(2)	0.19628(8)	0.0281(4)
S18	S _{1.00}	0.5775(3)	0.1029(2)	0.79103(9)	0.0352(4)

564

565 **Table 5.** Bond-valence balance (in valence unit, *vu*) in (Tl,As)-enriched boscardinite using the parameters proposed by Brese and O’Keeffe
 566 (1991).

	Tl1	Tl2a	Tl2b	Pb3a	Sb3b	Pb4a	Sb4b	Sb1	Sb2	As3a	As4	Sb5	Sb6	Sb7	As8	Sb9a	Pb9b	Sb10a	Ag10b	Σ anions
567 S1		0.02	0.06					0.60	0.16	0.08	1.02									1.94
568 S2				0.05	0.02							0.08	0.85	0.08 0.06	0.85					1.99
569 S3		0.06	0.04			0.42	0.16	0.17	0.26	0.99										2.10
570 S4	0.18	0.05	0.06	0.19	0.07	0.27	0.08					1.01								1.91
571 S5				0.03		0.11	0.01							0.86		0.78	0.01	0.26	0.06	2.12
572 S6													0.07	1.06	0.15	0.31 0.07	0.01	0.29	0.09	1.97
573 S7	0.13	0.11	0.10					0.92 0.81		0.11										2.18
574 S8	0.13	0.06	0.03	0.33	0.12	0.15	0.02						1.10							1.94
575 S9	0.13							0.85 0.03	0.07	0.06	0.93									1.94
576 S10												0.06		0.40 0.04	0.04	0.23	0.01	0.65 0.29	0.08 0.04	1.84
577 S11												0.06	0.24	0.51	1.08 0.05		0.01			1.95
578 S12	0.09	0.07	0.16					0.03	0.78		0.89 0.07									2.09
579 S13				0.06	0.01	0.13	0.01								0.92	0.65	0.03	0.06	0.05	1.92
580 S14		0.11	0.16			0.04						1.00	0.08			0.65	0.04			2.08
581 S15	0.14			0.44	0.13			0.38		0.99	0.04									2.12
582 S16	0.16			0.03								0.94	0.61					0.15	0.10	1.99
583 S17	0.11	0.06	0.24	0.12	0.02	0.27	0.09	1.02												1.93
584 S18	0.16	0.11	0.15	0.18	0.03	0.24	0.04			1.04										1.95
585 Σ cations	1.23	0.65	1.00	1.43	0.41	1.63	0.41	3.08	3.00	3.16	3.06	3.15	2.95	3.01	3.09	2.69	0.12	1.70	0.42	
586 Theor.*	1.10	0.59	0.80	1.51	0.72	1.62	0.57	3.00	3.00	3.00	3.00	3.00	3.00	3.00	3.00	2.87	0.09	1.80	0.40	

587

588 In mixed sites, bond-valence contribution of each cation has been weighted according to its occupancy (see Table 3).
 589

590 **Table 6.** Site occupancies in type boscardinite (Orlandi *et al.*, 2012) and in (Tl,As)-enriched
 591 boscardinite. Site labels agree with those given in Table 3. Average $\langle Me-S \rangle$ distances for
 592 (Sb/As) sites have been calculated considering bond distances shorter than 3.0 Å.
 593

Site	Orlandi <i>et al.</i> (2012)		this work	
	s.o.f.	$\langle Me-S \rangle$	s.o.f.	$\langle Me-S \rangle$
Tl1	Tl _{0.80} Pb _{0.20}	3.371	Tl _{0.90} Pb _{0.10}	3.367
Tl2a/Tl2b	Pb _{0.77} Tl _{0.23}	3.165/3.265	Tl _{0.61} Pb _{0.39}	3.282/3.295
Pb3a/Sb3b	Pb _{0.80} Tl _{0.20}	3.315	Pb _{0.76} Sb _{0.24}	3.276/2.77
Pb4a/Sb4b	Pb _{1.00}	3.136	Pb _{0.81} Sb _{0.19}	3.133/2.667
Sb1	Sb _{1.00}	2.601	Sb _{1.00}	2.600
Sb2	Sb _{1.00}	2.617	Sb _{1.00}	2.626
As3	Sb _{0.71} As _{0.29}	2.408	As _{0.60} Sb _{0.40}	2.345
As4	As _{0.75} Sb _{0.25}	2.334	As _{0.87} Sb _{0.13}	2.311
Sb5	Sb _{0.78} As _{0.22}	2.415	Sb _{0.51} As _{0.49}	2.378
Sb6	Sb _{1.00}	2.619	Sb _{0.73} As _{0.27}	2.592
Sb7	Sb _{1.00}	2.617	Sb _{1.00}	2.606
As8	Sb _{0.53} As _{0.47}	2.395	As _{0.63} Sb _{0.37}	2.363
Sb9a/Pb9b	Sb _{0.81} Pb _{0.19}	2.646/2.975	Sb _{0.96} Pb _{0.04}	2.712/2.967
Sb10a/Ag10b	Sb _{0.71} Ag _{0.29}	2.728/2.847	Sb _{0.60} Ag _{0.40}	2.713/2.826

594

595

596 **Table 7.** Proposed site occupancies at mixed (Tl/Pb) sites. Site occupancies calculated
 597 according to the bond-valence parameter $R_{Tl,S}$ proposed by Brese and O'Keeffe (1991) (B &
 598 O) and by Biagioni *et al.* (2014a) (B *et al.*).

Type boscardinite				(Tl,As)-enriched boscardinite			
Orlandi <i>et al.</i> (2012) – $\Sigma Ti_{EPMA} = 1.23$ (# 4977)				this work – $\Sigma Ti_{EPMA} = 1.52$ (# 1)			
Site	B & O	B <i>et al.</i>	Proposed	Site	B & O	B <i>et al.</i>	Proposed
(Tl,Pb)1	Tl _{0.81} Pb _{0.19}	Tl _{1.00}	Tl _{0.80} Pb _{0.20}	Tl1	Tl _{0.80} Pb _{0.20}	Tl _{0.99} Pb _{0.01}	Tl _{0.90} Pb _{0.10}
(Pb,Tl)2a	Pb _{0.27} Tl _{0.11}	Pb _{0.22} Tl _{0.16}	Pb _{0.27} Tl _{0.11}	Tl2a	Pb _{0.24} Tl _{0.17}	Tl _{0.22} Pb _{0.19}	Tl _{0.23} Pb _{0.18}
(Pb,Tl)2b	Pb _{0.48} Tl _{0.12}	Pb _{0.42} Tl _{0.20}	Pb _{0.50} Tl _{0.12}	Tl2b	Tl _{0.30} Pb _{0.29}	Tl _{0.39} Pb _{0.20}	Tl _{0.38} Pb _{0.21}
(Pb,Tl)3	Pb _{0.79} Tl _{0.21}	Pb _{0.70} Tl _{0.30}	Pb _{0.80} Tl _{0.20}				
ΣTi	1.25	1.66	1.23	ΣTi	1.27	1.60	1.51

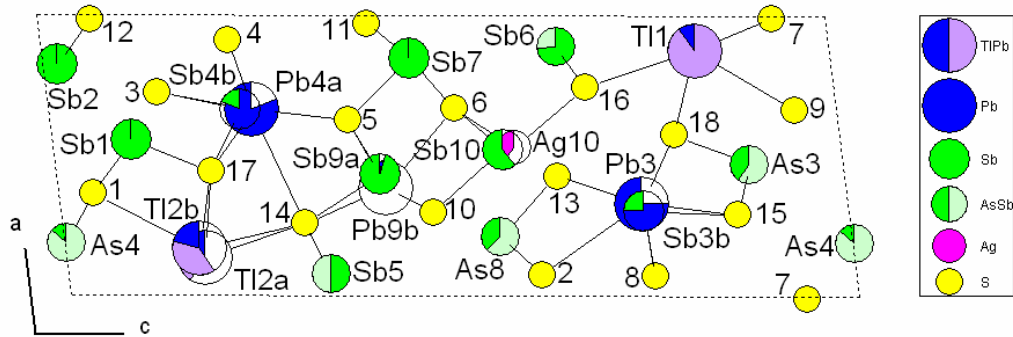
599

600

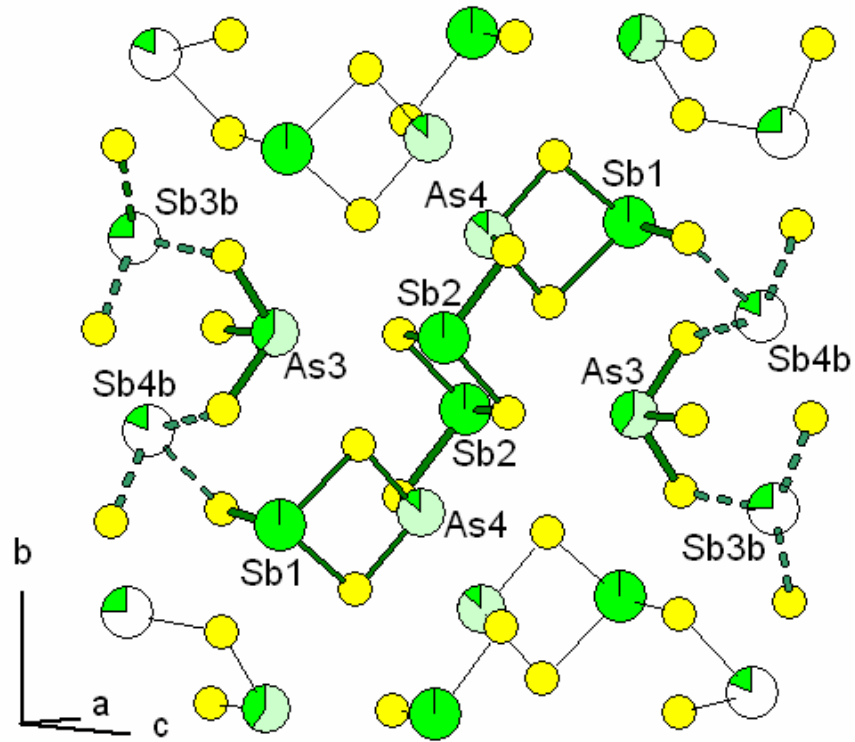
601 **Figure 1.** Crystal structure of (Tl,As)-enriched boscardinite as seen down **b**. Numbers without
 602 specification refer to S sites.

603

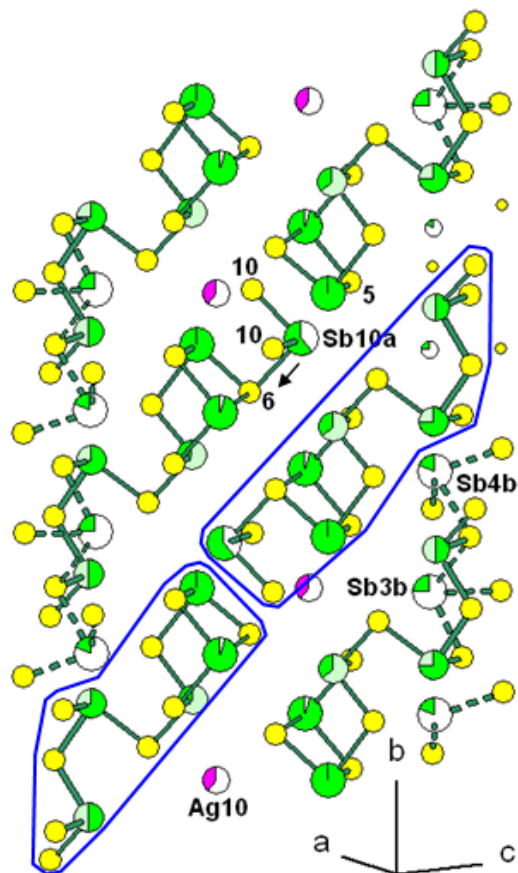
604



605 **Figure 2.** Polymerization within the sartorite layer of (Tl,As)-enriched boscardinite.
606
607

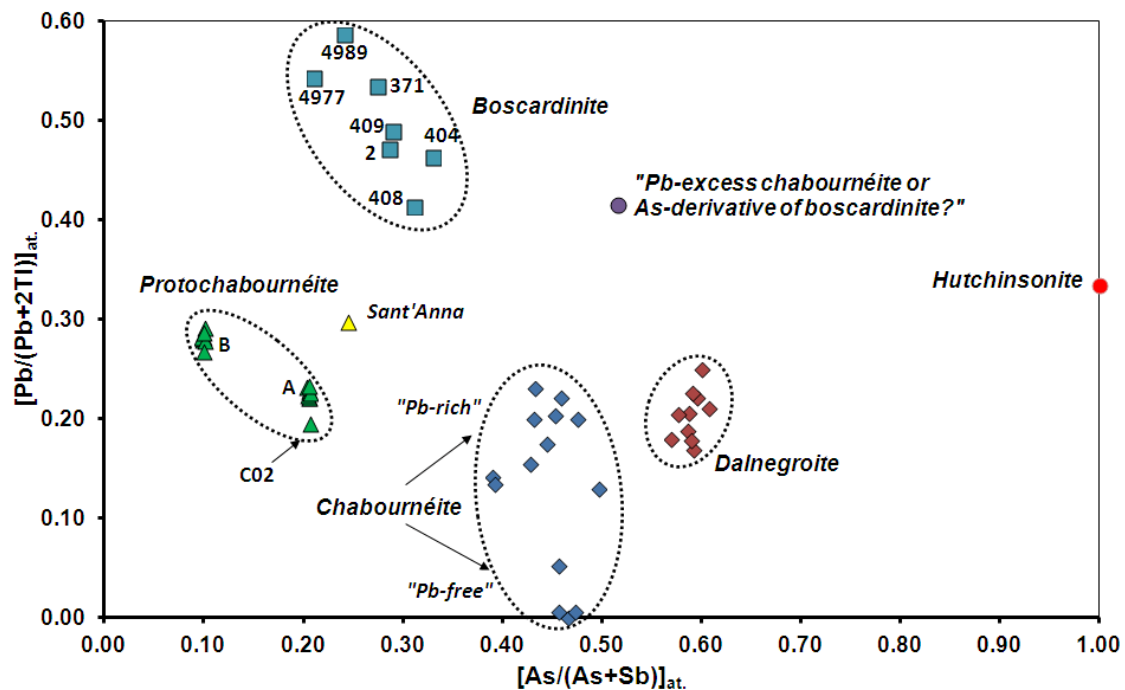


608 **Figure 3.** Main polymerization scheme (proposal) within the dufrénoysite layer of (Tl,As)-
 609 rich boscardinite (Pb9b absent, Sb10a alternation with Ag10b). Blue lines enclose the two
 610 polymers $\text{Sb}_3(\text{Sb,As})_2(\text{As,Sb})\text{S}_{11}$ and $\text{Sb}_2(\text{Sb,As})_2(\text{As,Sb})\text{S}_9$. Black arrow: shift of Sb10a
 611 towards S6 (a shift towards S5 is equiprobable).



612
 613

614 **Figure 4.** As/(As+Sb) versus Pb/(Pb+2Tl) atomic ratio in the chabournéite series and in
 615 boscardinite. Lozenges: chabournéite (data after Mantiene, 1974; Johan *et al.*, 1981; Shimizu
 616 *et al.*, 1999; Biagioni *et al.*, 2015; D. Harris, writ. commun., 1989) and dalnegroite (Nestola
 617 *et al.*, 2009). Triangles: protochabournéite (A and B correspond to analyses given in Orlandi *et*
 618 *al.*, 2013). Square: boscardinite (4977 and 4989 correspond to analyses of type boscardinite
 619 given in Orlandi *et al.*, 2012; the remaining analyses are discussed in the text). Circles: “Pb-
 620 excess chabournéite derivative or As-boscardinite derivative (data after Johan *et al.*, 1981)
 621 and ideal chemical composition of hutchinsonite, $TlPbAs_5S_9$.



622

